Original Article

Magnetic resonance tractography of the brachial plexus: step-by-step

Ibrahim Ibrahim[1]^, Antonín Škoch[1]^, Vít Herynek[2]^, Ivan Humhej[3]^, Jan Beran[1], Vlasta Flusserová[1], Eva Rolencová[1], Martina Juhaňáková[1], Michal Brzák[1], Markéta Nagy[1], Jaroslav Tintěra[1]^

[1]Department of Diagnostic and Interventional Radiology, Institute for Clinical and Experimental Medicine, Prague, Czech Republic; [2]Center for Advanced Preclinical Imaging, First Faculty of Medicine, Charles University, Prague, Czech Republic; [3]Department of Neurosurgery, J. E. Purkyně University, Masaryk Hospital, Ústí nad Labem, Czech Republic

Contributions: (I) Conception and design: I Ibrahim, J Tintěra; (II) Administrative support: I Humhej, J Beran; (III) Provision of study materials or patients: V Flusserová, M Juhaňáková, M Brzák; (IV) Collection and assembly of data: I Ibrahim, E Rolencová, M Nagy, J Tintěra; (V) Data analysis and interpretation: I Ibrahim, A Skoch, V Herynek; (VI) Manuscript writing: All authors; (VII) Final approval of manuscript: All authors.

Correspondence to: Ibrahim Ibrahim. Department of Diagnostic and Interventional Radiology, Institute for Clinical and Experimental Medicine, Videnska 1958/9, Prague 14021, Czech Republic. Email: ibib@ikem.cz.

Background: Magnetic resonance (MR) tractography of the brachial plexus (BP) is challenging due to different factors such as motion artifacts, pulsation artifacts, signal-to-noise ratio, spatial resolution; eddy currents induced geometric distortions, sequence parameters and choice of used coils. Notably challenging is the separation of the peripheral nerve bundles and skeletal muscles as both structures have similar fractional anisotropy values. We proposed an algorithm for robust visualization and assessment of BP root bundles using the segmentation of the spinal cord (SSC, C4-T1) as seed points for the initial starting area for the fibre tracking algorithm.

Methods: Twenty-seven healthy volunteers and four patients with root avulsions underwent magnetic resonance imaging (MRI) examinations on a 3T MR scanner with optimized measurement protocols for diffusion-weighted images and coronal T2 weighted 3D short-term inversion recovery sampling perfection with application optimized contrast using varying flip angle evaluation sequences used for BP fibre reconstruction and MR neurography (MRN). The fibre bundles reconstruction was optimized in terms of eliminating the skeletal muscle fibres contamination using the SSC and the tracking threshold of the normalized quantitative anisotropy (NQA) on reconstruction of the BP. In our study, the NQA parameter has been used for fiber tracking instead of fractional anisotropy (FA). The diffusion data were processed in individual C4-T1 root bundles using the generalized q-sampling imaging (GQI) algorithm. Calculated diffusion parameters were statistically analysed using the two-sample *t*-test. The MRN was performed in MedINRIA and post-processed using the maximum intensity projection (MIP) method to demonstrate BP root bundles in multiple planes.

Results: In control subjects, no significant effect of laterality in diffusion parameters was found (P>0.05) in the BP. In the central part of the BP, a significant difference between control subjects and patients at P=0.02 was found in the NQA values. Other diffusion parameters were not significantly different.

Conclusions: Using NQA instead of FA in the proposed algorithm allowed for a better separation of muscle and root nerve bundles. The presented algorithm yields a high quality reconstruction of the BP bundles that may be helpful both in research and clinical practice.

^ ORCID: Ibrahim Ibrahim, 0000-0003-3530-5165; Antonín Škoch, 0000-0002-1739-3256; Vít Herynek, 0000-0002-1775-2394; Ivan Humhej, 0000-0002-3971-2625; Jaroslav Tintěra, 0000-0002-0685-7174.

Keywords: Diffusion tensor imaging (DTI); brachial plexus; magnetic resonance neurography (MRN); magnetic resonance tractography (MRT); generalized q-sampling imaging algorithm (GQI algorithm)

Submitted Jan 11, 2022. Accepted for publication Jun 06, 2022.
doi: 10.21037/qims-22-30
View this article at: https://dx.doi.org/10.21037/qims-22-30

Introduction

The brachial plexus (BP) represents a complex neural structure that provides motor and sensitive innervation of the upper extremity. The BP is formed by the ventral rami of the lower four cervical roots (C5–C8) and comprises of roots, trunks, divisions, cords, and terminal branches (five nerves: axillary, musculocutaneous, radial, ulnar and median nerves) (1). Lesions of the BP are among the most serious disabilities ever, given its importance to the upper limb function. Brachial plexus injury is one of the most common injury in young people of working age, causing socio-economic problems and psychiatric disorders (2). The most common causes of BP affections are traffic accidents and sports injuries (3), compressive syndromes [thoracic outlet syndrome (TOS), carpal tunnel and cubital tunnel syndromes (4-6)], tumours, iatrogenic lesions, acute plexitis, post-radiation plexopathy and brachial plexopathy due to arterial aneurysms (7,8). The diagnosis of brachial plexopathy and upper limb neuropathy may pose a particular problem for the clinician and neurologist in terms of the location and extent of lesions, or in determining the type and etiology of the disease. In order to achieve the best therapeutic results in dealing with the above-mentioned affections, we need a thorough knowledge of anatomy, useful in clinical examination, interpretation of imaging methods, as well as possible operational intervention. The development of imaging methods and advances in the field of neuroscience have opened up new possibilities in exploring peripheral nerves (PN), and provide much of the core information influencing the diagnosis accuracy and treatment plan for these severe disabilities (9,10).

Brachial plexopathies and neuropathies of the upper extremity are best displayed by magnetic resonance imaging (MRI), which provides excellent contrast of soft tissues and detailed anatomical structures in any plane using advanced magnetic resonance (MR) techniques including structural 3D MR neurography (MRN), diffusion-weighted imaging (DWI), diffusion tensor imaging (DTI), and MR tractography (MRT) (11-14).

MRN is a method that provides an excellent evaluation of 3D anatomy of peripheral nerves using two- and three-dimensional imaging sequences with high resolution, which enable optimization of the contrast between the nerves and surrounding tissues. Furthermore, maximum intensity projection method (MIP) can be used for post processing of the 3D images to highlight nerve abnormalities (signal changes, continuity, nerve enlargement and compression, presence of intrinsic or extrinsic tumors) and tissues in their surroundings (muscle signal changes consistent with denervation, muscle atrophy, presence of pseudomeningocele in nerve root avulsions, haematomas, etc.) and to illustratively demonstrate peripheral nerve tracts in multiple planes (15,16). While playing a crucial role in examining the peripheral neuropathies, conventional and advanced MRN techniques cannot provide any information about the state of the nerve tracts in terms of their function. However, MR methods based on diffusion measurement (DWI, DTI, and MRT) may enable the evaluation of these functional properties. Also, diffusion kurtosis imaging (DKI), which quantifies the leading deviation from Gaussian diffusion, is sensitive to the tissue microstructure (17) and has already been used for tractography in experimental animals (18). These methods enable evaluation of the microstructure of axonal bundles and identification of the degeneration or regeneration (19-21) of brachial plexopathies and neuropathies of the upper extremity based on diffusion properties of the PN tissue. DTI and MRT are MRI techniques based on DWI, which enable to quantitatively evaluate neuronal fibres in 2D and 3D images, and to visualize them. The brachial plexopathies can alter the integrity of fibre tracts, which cause the changes detectable by DTI. The alterations are mainly reflected in DTI-based metrics such as fractional anisotropy (FA) and mean diffusivity (MD) (22,23), and metrics based on generalized q-sampling imaging (GQI), such as quantitative anisotropy (QA) (24). Fractional anisotropy is the most important diffusion index that describes the extent to which diffusion is directionally restricted whereas MD

Table 1 Sequence parameters used for high-resolution MRN, and diffusion-weighted single-shot echo-planar imaging sequence used for BP fibre reconstruction

Sequence parameters	3D STIR SPACE	ss-EPI
Repetition time (ms)	1,500	7,500
Echo time (ms)	100	79
Echo spacing (ms)	3.58	0.69
Inversion time (ms)	200	–
b-value 1/2 (s/mm^2)	NA	0/800
In-plane resolution (mm^2)	1×1	3×3
Orientation	Coronal	Transversal
No. of slices	160	66
Bandwidth (Hz/Px)	592	2,790
Parallel acquisition technique (GRAPPA)	2	2
Field of view (mm^2)	384×384	384×264
No. of gradient directions	NA	64
No. of signal averages	1	2
Total scan time (min)	10:00	8:32

MRN, magnetic resonance neurography; BP, brachial plexus; ss-EPI, single-shot echo-planar imaging sequence; STIR, short tau inversion recovery; SPACE, sampling perfection with application of optimized contrast using different flip angle evolution; GRAPPA, generalized autocalibrating partial parallel acquisition; NA, not applicable.

represents a quantitative metric of average molecular diffusion of water in the imaged voxel. QA measures the density of anisotropy diffusion along a fibre pathway. QA is defined for each resolved fiber orientation, robust against peritumoral edema, and is less sensitive to the partial volume effect of free water and crossing fibers (25-27). Therefore, QA may serve as a good indicator of nerve damage (25,28). Decreased QA values may indicate damage of nerve fibers (degeneration, demyelination, neuronal injury), while higher values may reflect the good condition of neuronal fibers. Normalized quantitative anisotropy (NQA) normalizes proton density between subjects. NQA is also robust against inflammation and edema (26).

Although numerous studies dealing with PN imaging have been performed using DWI, DTI and MRT (29-32), these diffusion-based methods are not standard part of clinical protocols used in peripheral nerve imaging yet.

MRT of the brachial plexus is demanding for the operator's skilfulness, sensitive to operator-dependent bias and time consuming. No standard method for data post-processing and MRT reconstruction techniques for the brachial plexus has been established yet. Nevertheless, the information they provide is of high importance for clinical practice. Therefore, we would address the possibility of standardizing the entire post-processing procedure to make it more feasible in clinical use. The goal of the study is to optimize, improve and propose a simple, fast, and robust algorithm for neuronal pathways reconstruction of the brachial plexus in control subjects and patients with brachial plexopathies and neuropathies of the upper extremity using qualitative and quantitative advanced MRI methods including MRN and MRT, and to implement them in clinical practice. We present the following article in accordance with the TRIPOD reporting checklist (available at https://qims.amegroups.com/article/view/10.21037/qims-22-30/rc).

Methods

MRI acquisition

Twenty seven healthy volunteers (3 females, 24 males, mean age of 34.85±8.98 years, range 19–51 years) and 4 patients with BP nerve root avulsions (males, mean age of 34.00±4.74, range 31–42 years) were included in this study. We used a 3T MR scanner (Siemens Trio TIM 3T, Erlangen, Germany) equipped with a 12-channel head coil and a 12-channel phased-array body coil. All subjects were scanned in the supine position and a following optimized protocol was used: (I) diffusion-weighted images acquired by the single-shot echo-planar imaging (ss-EPI) sequence used for BP fiber reconstruction; and (II) coronal T2 weighted 3D short-term inversion recovery (STIR) SPACE (sampling perfection with application optimized contrast using varying flip angle evaluation) sequence used for high-resolution MRN. All sequence parameters are summarized in *Table 1*. In patients, additional imaging sequences were used to identify and confirm the diagnosis of BP disorders [e.g., standard sagittal 2D T2-weighted turbo spin-echo (TSE) sequence with TR/TE: 3,500/99 ms and field of view (FOV) of 384 mm × 384 mm].

All healthy subjects had no relevant medical history and they were asymptomatic. MR data were checked by two radiologists with more than 30 years of professional experience. The study was conducted in accordance with the Declaration of Helsinki (as revised in 2013). Both healthy subjects and patients were informed about the purpose of the study prior to the examination, and signed their written

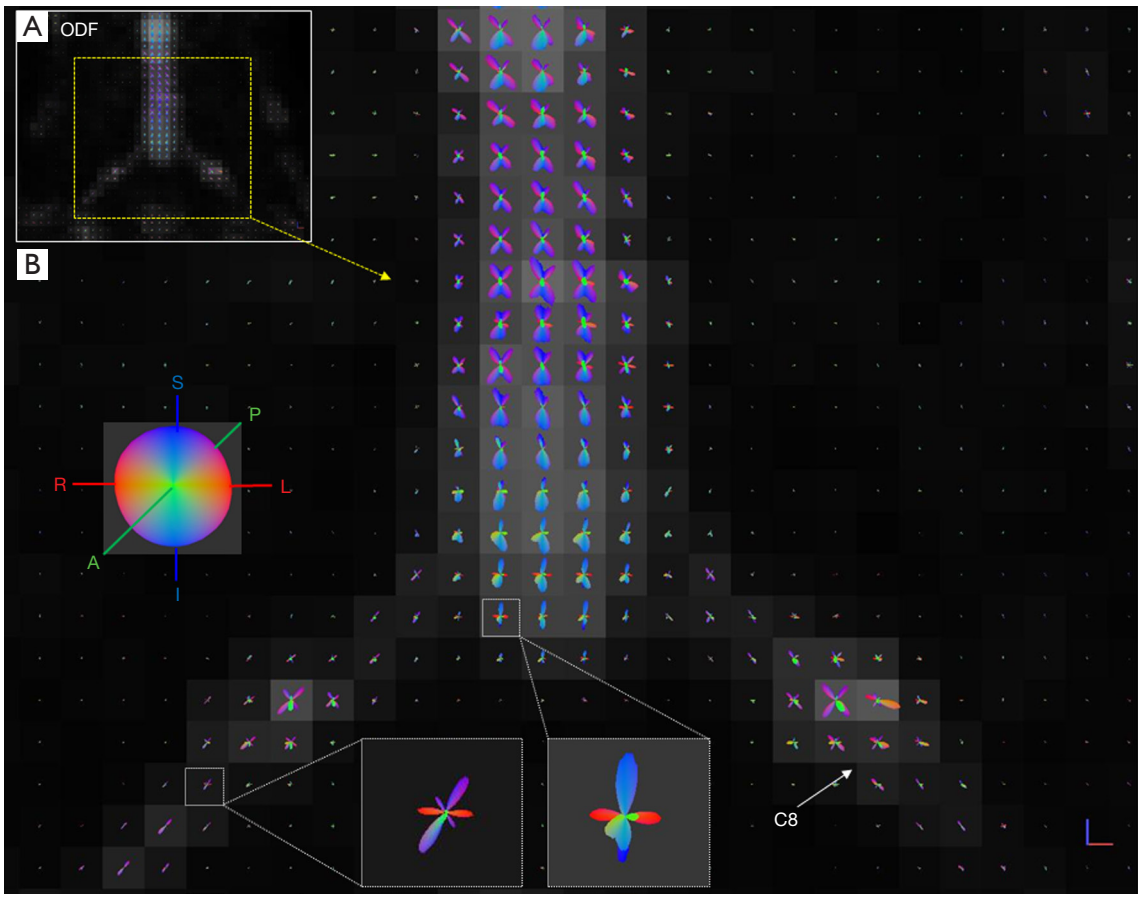

Figure 1 The diffusion ODF obtained from q-sampling imaging. (A) The ODF map; (B) details of zoomed voxels with ODF shape and orientations of multiple fibre population. The directions of the ODF are pseudo-colored: red in the left-right direction (L-R), blue in the superior-inferior direction (S-I), and green in the anterior-posterior (A-P) direction. ODF, orientation distribution function.

consent. The study (including the measurement protocol) was approved by the ethics committee of the Institute for Clinical and Experimental Medicine and Thomayer Hospital (No. G-16-06-08).

Data processing

Correction of distorsions and effects caused by eddy currents in the diffusion data was performed using an eddy tool (a function implemented in FSL software, https://www.ncbi.nlm.nih.gov/pubmed/26481672). Then we reconstructed the diffusion data using the DSI studio (freeware tool for MRT, http://dsi-studio.labsolver.org) with the GQI and the deterministic fibre tracking algorithm was used (33). GQI is a model-free reconstruction technique that can be applied to any diffusion sampling scheme, and provides a QA parameter based on the spin distribution function (SDF) (24,34). SDF defines the diffusion water density in different orientations, determined by the high order models for estimating voxels with multiple fiber populations (*Figure 1*).

Optimization of the BP bundles reconstruction included elimination of the skeletal muscle fibers (especially scalene muscles) contamination using the effects of the NQA and determination of angular threshold for BP fiber bundle reconstruction (*Figure 2*) (35).

The workflow is described in the block scheme (*Figure 3*). The final algorithm contains following steps (*Figure 4*).

Firstly, the spinal cord (SC) was manually segmented (C4-T1) from the corrected NQA images using a Wacom Cintiq 22 drawing tablet (*Figure 4A*). The segmented SC was then used as a set of seed points for reconstruction of the major pathway roots of the brachial plexus. Two additional regions of interest (ROIs) were used as terminative regions

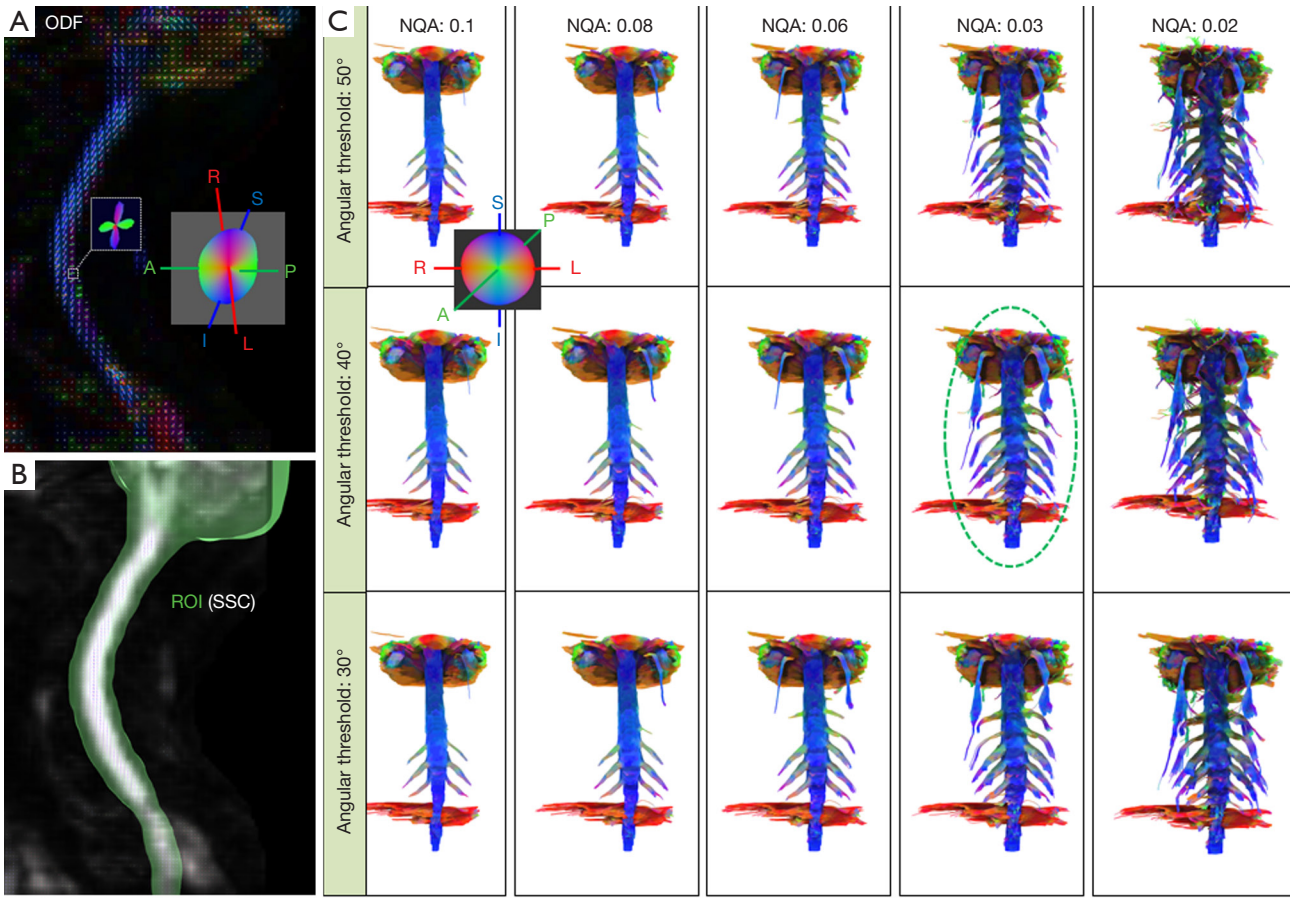

Figure 2 Effects of the NQA and angular threshold on the reconstruction of the fibre bundles. (A) Sagittal view; (B) SSC used as a ROI for the initial starting area for the fiber tracking algorithm; (C) the dependency of fiber tracking results on the NQA (e.g., 0.1) and angular thresholds; multiple fiber bundles (C4-T1) are visible with a decreasing NQA threshold. The best reconstruction (green circled image) of the brachial plexus requires an NQA threshold 0.03 (or 0.02) and angular threshold 30° to 50° (two last columns). Directional colors show the local orientation of the ODF and the fiber tracts: red in the left-right direction (L-R), blue in the superior-inferior direction (S-I), and green in the anterior-posterior (A-P) direction. NQA, normalized quantitative anisotropy; ODF, orientation distribution function; SSC, segmented spinal cord; ROI, region of interest.

that do not allow a tract to pass through them. One of those regions was set proximally (ROI-1) at the level of the C3/C4 intervertebral disk and the other (ROI-2) was set distally at the level of the T1/T2 intervertebral disk (*Figure 4A*,*4B*). To minimize the contamination by the scalene muscle fibers, an algorithm implemented in DSI studio for deterministic streamline fiber tracking was used. We used following tracking parameters: NQA was 0.03, the angular threshold was 40°, the step size was 1 mm. The primary orientation and subvoxel seeding were set to visualize the major fiber roots of the brachial plexus (*Figure 4A*,*4B*). A total of 1,000,000 seeds were chosen at random subvoxel positions; the number of seed points was set to be safely beyond the required number for reliable track visualization (20).

Secondly, the right (*Figure 4C*,*4D*) and left (*Figure 4E*,*4F*) brachial plexus (C4-T1), and the central part (*Figure 4G-4J*) of the cervical spinal cord (without the roots) were separately selected from the reconstructed BP using the DSI studio with the shortcuts for track selection or tract deleting in the 3D window as follows:

(I) To select the right BP (C4-T1), move the cursor to the starting point of the selection plane on the screen (*Figure 4C*);
(II) Press the keyboard shortcut Ctrl+S (selection of the tracts in the 3D window);
(III) Press the left button of the mouse and drag the

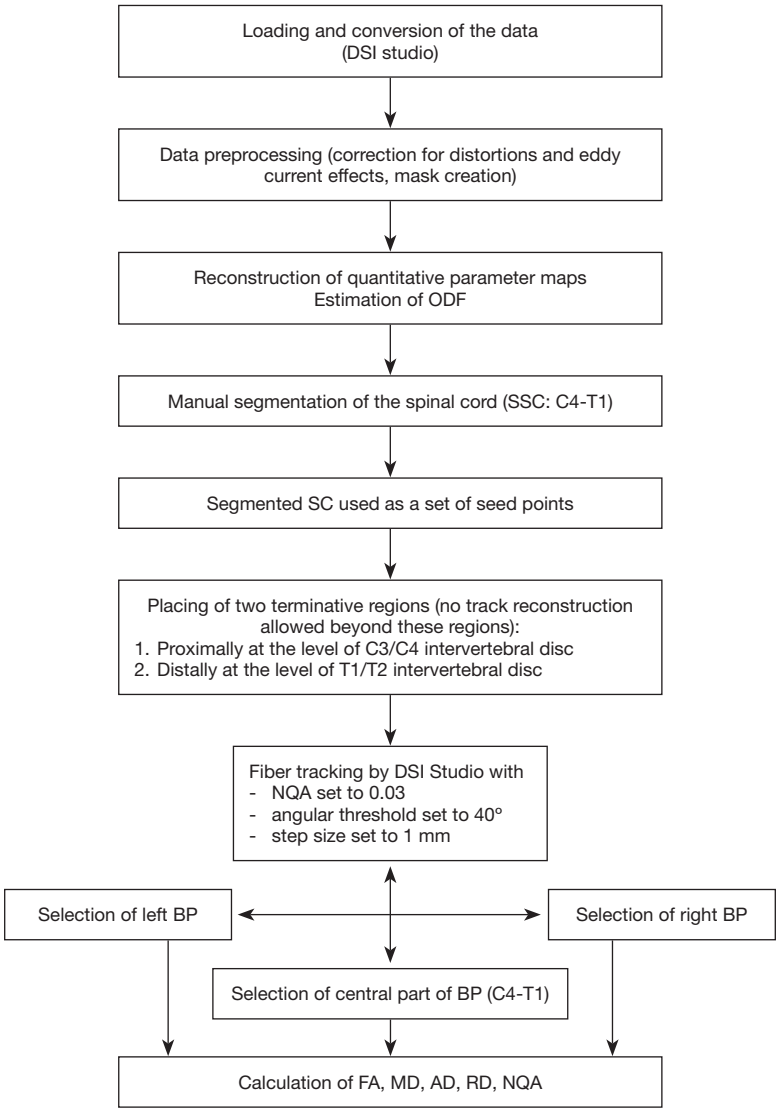

Figure 3 A block scheme of the fiber tracking workflow describing the proposed algorithm for magnetic resonance tractography of the BP. BP, brachial plexus; ODF, orientation distribution function; FA, fractional anisotropy; MD, mean diffusivity; AD, axial diffusivity; RD, radial diffusivity; NQA, normalized quantitative anisotropy; DSI Studio, freeware tool for magnetic resonance tractography; SSC, segmented spinal cord; SC, spinal cord.

cursor to the ending point of the selection plane (*Figure 4C*,*4D*);

(IV) Release the button and the selection will be performed immediately (*Figure 4D*);

(V) Repeat the same steps (1 to 4) to select the left BP (*Figure 4E*,*4F*);

(VI) To select the central part of BP without roots, repeat the same steps (1 to 4) with the keyboard shortcut Ctrl + D instead of Ctrl + S. The result of BP reconstruction is shown in *Figure 4G-4J*.

The selected parameters (i.e., NQA, angular threshold, etc.) are constant across all subjects.

The proposed algorithm was applied to all subjects and the locations of the ROIs were precisely defined by the cervical and thoracic intervertebral discs (C3/C4 and T1/T2). The reconstruction procedure is time consuming; generation of the full tractogram takes 25–30 min. A software MedINRIA (http://med.inria.fr/) was used for reconstruction of MRN images. Maximum intensity projection was used for image enhancement.

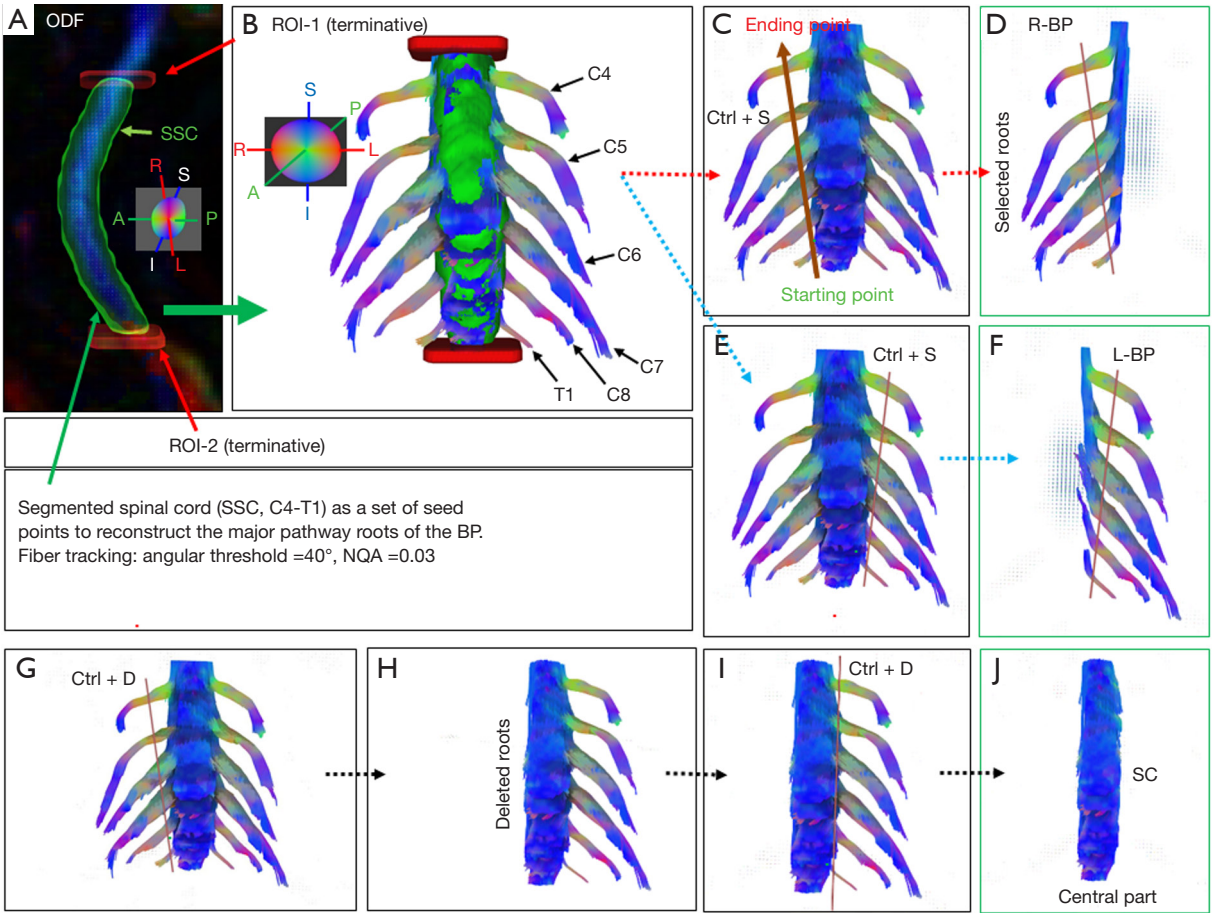

Figure 4 Reconstruction of the root bundles C4-T1 in detail in a 24-year-old healthy man. Figure parts (A) to (J) show individual reconstruction steps: (A) SSC was used as seed points for the initial starting area for the fibre tracking algorithm within these seeding regions at subvoxel resolution; (B) reconstruction of the major pathway roots of the right BP (C4-T1) using the SSC with NQA of 0.03 and angular thresholding of 40°; (C,D) selection of the right BP using shortcut Ctrl + S; (E,F) selection of the left BP; (G-J) central part BP selection using shortcut Ctrl + D. Directional colors show the local orientation of the orientation distribution function and the fiber tracts: red in the left-right direction (L-R), blue in the superior-inferior direction (S-I), and green in the anterior-posterior (A-P) direction. SSC, segmented spinal cord; BP, brachial plexus; ODF, orientation distribution function map; ROI, regions of interest; L, left; R, right; SC, spinal cord; NQA, normalized quantitative anisotropy.

Mean values of the DTI-based metrics [FA, MD, axial diffusivity (AD), and radial diffusivity (RD)], and GQI-based-metrics (NQA), measured based on restricted diffusion of the root bundles were evaluated in each subject in both sides of BP (C4-T1) separately (right BP and left BP, referred to as laterality below; *Table 2*), and also for the central part of BP without roots (*Figure 4*, *Table 3*).

Statistical analysis

To evaluate the dependency of DTI/GQI-based metrics (FA, AD, RD and MD/NQA) on laterality, diffusion metrics of healthy controls in both BP sides were compared using paired *t*-tests.

The above-mentioned parameters were also calculated in the central part of the spinal cord (*Figure 4J*) in four patients with root avulsions and compared to the results of 27 control subjects using two-sample *t*-tests with equal variances. Homogeneity of variance was tested by F-tests. The P values were adjusted for multiple comparisons using the Holm method (36) (http://www.jstor.org/stable/4615733).

Table 2 Quantitative diffusion analysis, comparison of the left and right BP in controls

Control subjects (n=27)	Left BP (C4-T1)		Right BP (C4-T1)		P value
	Mean ± SD	Coef. of variation, %	Mean ± SD	Coef. of variation, %	
NQA	0.09±0.03	33.3	0.1±0.02	20.0	0.07
FA	0.25±0.02	8.00	0.25±0.03	12.0	0.07
MD (10^{-3} mm^2/s)	1.97±0.21	10.7	1.97±0.27	15.1	0.09
AD (10^{-3} mm^2/s)	2.42±0.25	10.3	2.46±0.29	11.8	0.53
RD (10^{-3} mm^2/s)	1.71±0.29	17.0	1.73±0.26	15.0	0.71

The results of calculated GQI/DTI-based metrics (NQA, FA, MD, AD, and RD) in the left and right hand side of the brachial plexus (C4-T1) are listed with their standard deviations. BP, brachial plexus; NQA, normalized quantitative anisotropy; FA, fractional anisotropy; MD, mean diffusivity; AD, axial diffusivity; RD, radial diffusivity; GQI, generalized q-sampling imaging; DTI, diffusion tensor imaging.

Table 3 Quantitative diffusion analysis, comparison of the central part of the BP in patients and controls

The central part of the BP (C4-T1)	Patients (n=4)		Control subjects (n=27)		P value
	Mean ± SD	Coef. of variation, %	Mean ± SD	Coef. of variation, %	
NQA	0.19±0.04	21.1	0.29±0.06	20.7	0.02
FA	0.31±0.03	9.7	0.33±0.04	12.1	ns
MD (10^{-3} mm^2/s)	2.21±0.27	12.2	2.18±0.25	11.5	ns
AD (10^{-3} mm^2/s)	2.88±0.32	11.1	2.89±0.25	8.7	ns
RD (10^{-3} mm^2/s)	1.88±0.26	13.8	1.83±0.25	13.7	ns

The results of calculated GQI/DTI-based metrics (NQA, FA, MD, AD, and RD) in the central part of the BP are listed with their standard deviations. BP, brachial plexus; ns, not significant; NQA, normalized quantitative anisotropy; FA, fractional anisotropy; MD, mean diffusivity; AD, axial diffusivity; RD, radial diffusivity; GQI, generalized q-sampling imaging; DTI, diffusion tensor imaging.

Results

The proposed algorithm efficiently tracked C4–T1 nerve roots in all subjects and proved to be robust. Demographic data of the subjects had no infuence on the tracking successfulness of the nerve roots.

Robustness of the method is demonstrated in *Figure 5*, which shows neurography and diffusion images of a healthy subject and a patient with nerve root avulsions. MRT imaged the torn off nerve roots at C7, C87, and T1 positions and confirmed suspected avulsions.

While the proposed procedure utilizes NQA for tracking the nerve roots, the measurement also provides quantification of other DTI-based metrics, which supports the presumption, that NQA is the most sensitive parameter for a reliable tractography. The mean FA, MD, AD, RD, and NQA values were calculated in both left and right sides of the BP (*Table 2*), and in the central part of the BP in all examined subjects (*Table 3*). In control subjects, no significant effect of laterality in diffusion parameters was found (P>0.05) in the brachial plexus. However, in the central part of the BP, a significant difference between control subjects and patients at P=0.02 was found in NQA values. The results of the two-sample *t*-tests are depicted in graphical form in *Figure 6*. Other diffusion parameters were not significantly different.

Discussion

Up to date, there has been no gold standard protocol for diffusion data-acquisition or uniform algorithm for post-processing data and MRT techniques of the brachial plexus and other peripheral nerves. A common criterion of fiber tracking in all previous studies is the use of fractional anisotropy and placement of various inclusion/exclusion ROIs along the neural pathways (37-39).

However, the proximity of peripheral nerves and skeletal muscles, similar FA values of both tissues, spatial resolution,

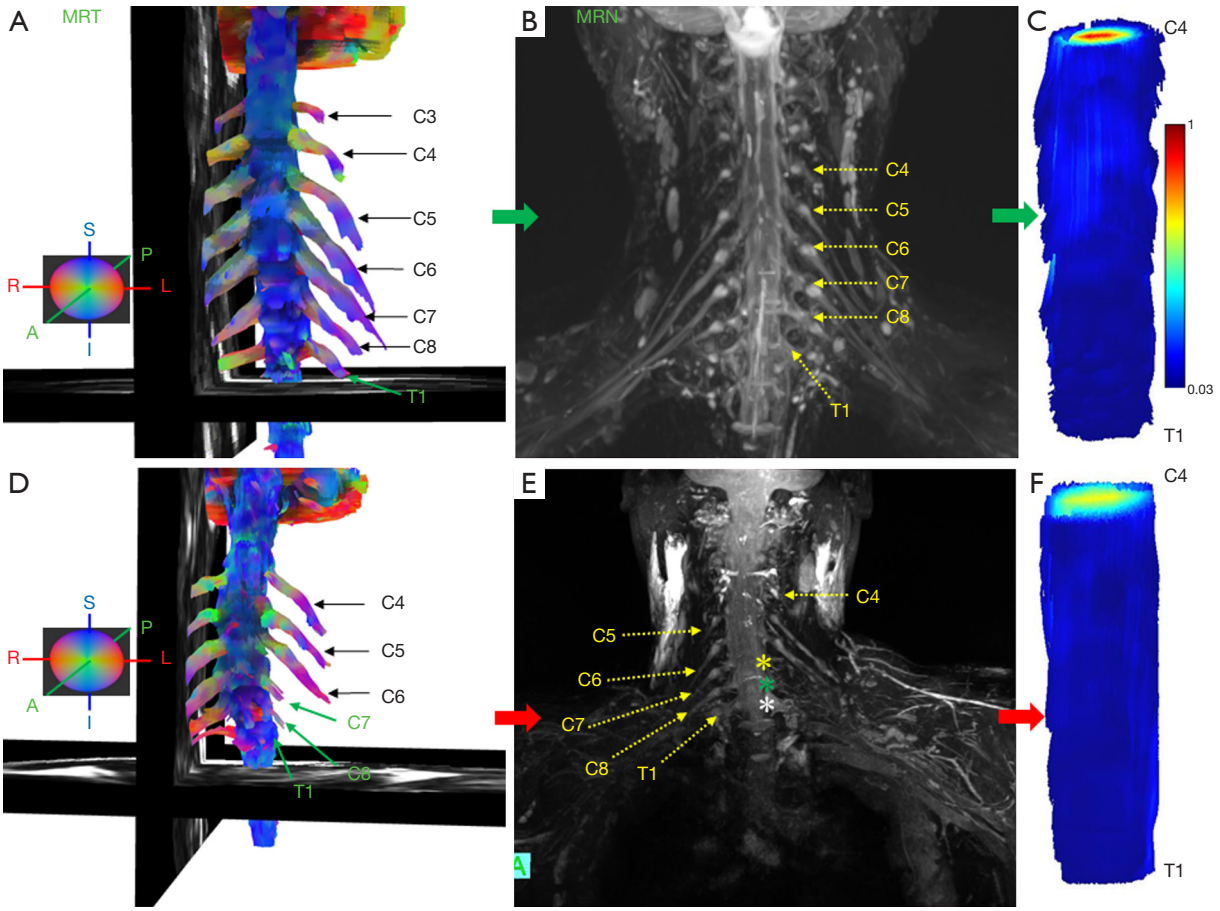

Figure 5 Representative MRT images and corresponding results of MRN reconstruction from a coronal 3D STIR SPACE images. (A) MRT acquired in a 25-year-old healthy man shows the architectural configuration of the reconstructed fibre bundles (C4-T1). (B) Corresponding MRN reconstruction. (C) The central part of the brachial plexus (C4-T1) of the healthy man. (D) MRT acquired in a 30-year-old patient with nerve root avulsions. (E) Corresponding MRN reconstruction. Three asterisks show nerve root avulsions (C7-T1). (F) The central part of the brachial plexus (C4-T1) of the patient. Directional colors (A, D) show the local orientation of fiber tracts: red in the left-right direction (L-R), blue in the superior-inferior direction (S-I), and green in the anterior-posterior (A-P) direction. The color coding of the magnitude of NQA in the central part of the brachial plexus shows color differences of fiber tracking results between a healthy subject (C) and a patient (F). MRT, magnetic resonance tractography; MRN, magnetic resonance neurography; NQA, normalized quantitative anisotropy; STIR, short-tau inversion recovery; SPACE, sampling perfection with application optimized contrast using varying flip angle evaluation.

algorithm type, different ROIs sizes, numbers and locations of the ROIs (40) may cause contamination by skeletal muscle fibers (e.g., scalene muscles), when MRT of the BP nerve bundles is performed.

In our study, in order to reduce the impact of skeletal muscle fibers on BP reconstruction, the NQA parameter has been used for fiber tracking (FT) instead of FA. The reason is that QA-aided tractography reached better resolution and is less sensitive to partial volume effects of crossing fibers than the tractography based on FA (33). QA measures the spin density (the amount of restricted diffusion) of anisotropy along a fiber pathway for each fiber population and is more robust against inflammation and edema, and contributes to more reliable tractography (41). FA is defined for all fiber populations within a voxel (none-restricted and restricted diffusion are always mixed) and suffers from the partial volume effect. In addition, QA can be normalized (NQA), which stabilizes the proton density across subjects. Our algorithm can be used in other procedures widely used for fiber tracking routines with the FA threshold, but for

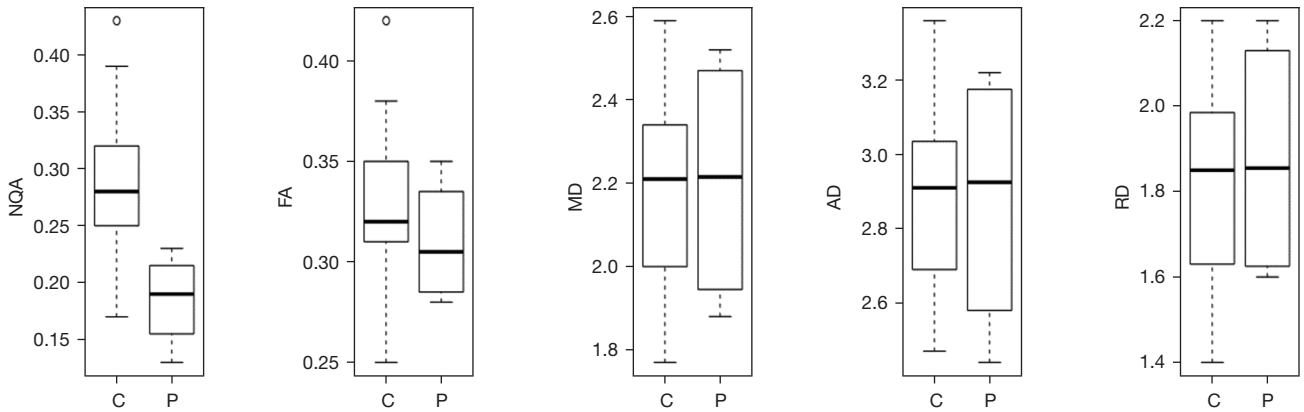

Figure 6 The results of the two-sample *t*-tests are depicted in graphical form (box plot) that shows a significant difference between control subjects and patients at P=0.02 in NQA values in the central part of the BP without root bundles (C4-T1). DTI-based metrics (FA, MD, AD, and RD) were not significantly different. NQA, normalized quantitative anisotropy; BP, brachial plexus; FA, fractional anisotropy; MD, mean diffusivity; AD, axial diffusivity; RD, radial diffusivity.

the above-mentioned reasons we recommend fiber tracking reconstructions with the NQA parameter. Our study thus for the first time reports on how to reconstruct the BP bundles using the segmentation of the spinal cord as the ROI, and with the optimized NQA thresholding. It should be noted that the selected angular threshold (30° to 50°) does not have much effect on the fiber reconstruction result (*Figure 2*). The proposed algorithm represents a robust, fast and straight-forward method for evaluation the BP, so it can be used by scientists, radiologists, neurologists, neurosurgeons and others without having much prior knowledge of the MRT methods. Representative MRN and MRT are shown in *Figure 5*.

The results of calculated diffusion—based metrics (FA, MD, AD, and RD) in the left and right hand side of the BP (C4-T1) with their standard deviations given in *Table 2* showed no significant effect of laterality in control subjects. These results correspond to already published results (42). Also, the NQA values of both sides are similar. However, in the central part of the BP, a significant difference between control subjects and patients at P=0.02 was found in the NQA values (*Figure 6*, *Table 3*). Other diffusion parameters were not significantly different. NQA is a sensitive parameter to pathological changes and indicates that there are some diffusion changes in the central part of the spinal cord of patients due to root avulsions.

MRT is challenging and successful fiber track reconstruction substantially depends on the quality of diffusion data. Many factors effect diffusion data quality, e.g., the presence and amount of motion and pulsation artifacts, also the signal-to-noise ratio and spatial resolution are very important factors. Eddy currents can induce geometric distortions. Naturally, also the sequence parameters and choice of used coils strongly influence final results (29). Notably challenging is the separation of the BP bundles and skeletal muscles as both structures have similar fractional anisotropy values (43). During the optimization of the algorithm, the combination of segmented spinal cord as seed points (ROI) and optimal NQA threshold setting as described in the method section has turned out to be key to accurately estimating the pathways of the fibres. Furthermore, the calculated diffusion parameters (e.g., FA, MD, AD and RD) and NQA can be used for evaluation of the integrity of the BP, and to show regeneration or degeneration of axons over time following nerve injuries. Also, the MRN method provides an excellent and accurate 3D anatomy of the peripheral nerves. However, MRN is challenging due to various factors such as insufficient suppression of vascular signals, spatial resolution, subject motion, insufficient fat-signal suppression and surrounding structures involved in the quality of the acquired data (44,45). With respect to this, the conventional 3D-T2-STIR MRN cannot visualize the neighboring vessels and therefore it cannot assess their involvement in brachial plexopathy.

Therefore, an accurate diagnosis of the disease requires simultaneous examination of the brachial plexus and its adjacent arteries/veins. Recent publications have shown that contrast-enhanced MRN can significantly improve the

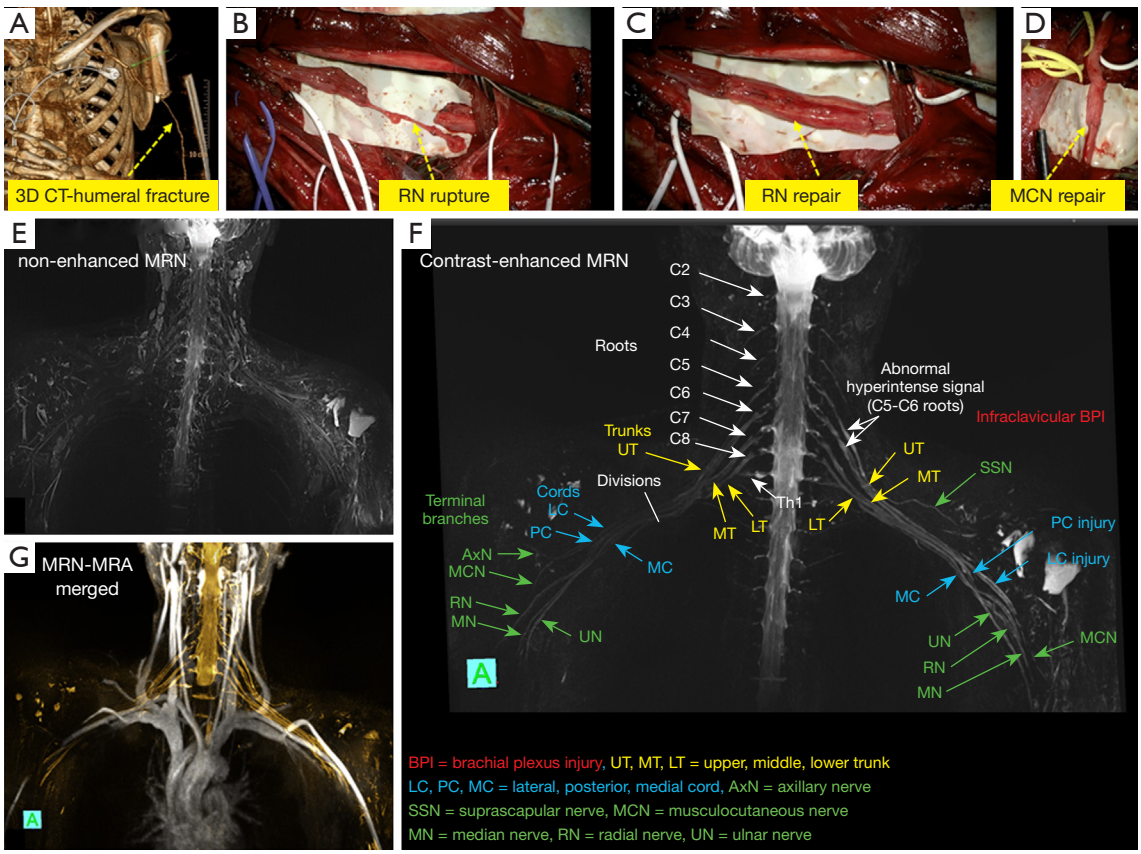

Figure 7 A representative contrast-enhanced MRN with MRA in a 37-year-old patient with left infraclavicular injuries of the brachial plexus. (A) The result of 3D CT of humeral fracture. (B-D) Neurosurgical reconstructions of RN and MCN. (E) The result of non-enhanced MRN. (F) Contrast-enhanced MRN. (G) Merged contrast-enhanced MRN and MRA images after neurosurgical reconstruction; it shows the benefit of contrast-enhanced MRN. MRN, magnetic resonance neurography; MRA, magnetic resonance angiography; CT, computed tomography; RN, radial nerves; MCN, musculocutaneus nerves.

visibility of peripheral nerves. It may also play a significant role in assessing brachial plexopathy and surrounding blood vessels using the combination of contrast-enhanced MRN and MR angiography (MRA) techniques (46-49).

Based on the two considerations referred to above, we presume that it would be beneficial to use a single dose of a contrast agent for acquisiton of both contrast-enhanced 3D-T2-STIR MRN (which better visualizes the brachial plexus), and contrast-enhanced MRA (for revealing of surrounding vessels). A representative contast-enhanced MRN with MRA in a patient with infraclavicular injuries (the patient underwent neurosurgical reconstruction of radial and musculocutaneus nerves) are shown in *Figure* 7.

A limitation of the study is a small sample size of patients; a study with a larger set is required to confirm our results showing diffusion changes in the central part of the spinal cord of patients with root avulsions. Another limitation is the absence of correlation of diffusion indices with EMG findings. Also, the NQA parameter is only used in the DSI studio, provided by the GQI-based metrics method.

It should also be noted that the combination of qualitative (MRN) and quantitative (MRT) techniques leads to a richer and more comprehensive understanding of peripheral nerves. In any case, our proposed algorithm is robust and can be used to assess the integrity of both normal and pathological BP nerves.

Conclusions

The proposed algorithm represents a very useful method for assessing both normal and pathological peripheral nerves. MRN and MRT have a potential to aid in decision-making in many neuropathies and plexopathies in terms of establishing correct diagnosis, conservative versus surgical treatment,

presurgical planning and post-operative follow-up.

Acknowledgments

We would like to thank Dr. Milan Hájek for proofreading the manuscript.
Funding: This study was supported by the Ministry of Health of the Czech Republic (Grant No. 17-28587A and No. IKEM, IN 00023001).

Footnote

Reporting Checklist: The authors have completed the TRIPOD reporting checklist. Available at https://qims.amegroups.com/article/view/10.21037/qims-22-30/rc

Conflicts of Interest: All authors have completed the ICMJE uniform disclosure form (available at https://qims.amegroups.com/article/view/10.21037/qims-22-30/coif). II, AŠ, IH, JB, MJ and JT report that this work was supported by scientific grants from the Ministry of Health of the Czech Republic (No. 17-28587A; No. IKEM, IN 00023001). The other authors have no conflicts of interest to declare.

Ethical Statement: The authors are accountable for all aspects of the work in ensuring that questions related to the accuracy or integrity of any part of the work are appropriately investigated and resolved. The study was conducted in accordance with the Declaration of Helsinki (as revised in 2013). All participants were informed about the purpose of the study and signed their written consent prior to the examination. The study were approved by the ethics committee of the Institute for Clinical and Experimental Medicine and Thomayer Hospital (No. G-16-06-08).

References

1. Bayot ML, Nassereddin A, Varacallo M. Anatomy, Shoulder and Upper Limb, Brachial Plexus. In: StatPearls. Treasure Island (FL): StatPearls Publishing, 2021.
2. Tharin BD, Kini JA, York GE, Ritter JL. Brachial plexopathy: a review of traumatic and nontraumatic causes. AJR Am J Roentgenol 2014;202:W67-75.
3. Luo TD, Levy ML, Li Z. Brachial Plexus Injuries. In: StatPearls. Treasure Island (FL): StatPearls Publishing, 2022.
4. Ohman JW, Thompson RW. Thoracic Outlet Syndrome in the Overhead Athlete: Diagnosis and Treatment Recommendations. Curr Rev Musculoskelet Med 2020;13:457-71.
5. Sharrak S, M Das J. Hand Nerve Compression Syndromes. In: StatPearls. Treasure Island (FL): StatPearls Publishing, 2021.
6. Davis DD, Kane SM. Ulnar Nerve Entrapment. In: StatPearls. Treasure Island (FL): StatPearls Publishing, 2021.
7. Gilcrease-Garcia BM, Deshmukh SD, Parsons MS. Anatomy, Imaging, and Pathologic Conditions of the Brachial Plexus. Radiographics 2020;40:1686-714.
8. Conroy M, Murphy LC, McNamara B, O'Reilly S. Delayed onset radiation-induced brachial plexopathy. Breast J 2020;26:2075-6.
9. Kwee RM, Chhabra A, Wang KC, Marker DR, Carrino JA. Accuracy of MRI in diagnosing peripheral nerve disease: a systematic review of the literature. AJR Am J Roentgenol 2014;203:1303-9.
10. Upadhyaya V, Choudur HN. Imaging in peripheral neuropathy: Ultrasound and MRI. Indian J Musculoskelet Radiol 2021;3:14-23.
11. Martín Noguerol T, Barousse R, Socolovsky M, Luna A. Quantitative magnetic resonance (MR) neurography for evaluation of peripheral nerves and plexus injuries. Quant Imaging Med Surg 2017;7:398-421.
12. Filler A. Magnetic resonance neurography and diffusion tensor imaging: origins, history, and clinical impact of the first 50,000 cases with an assessment of efficacy and utility in a prospective 5000-patient study group. Neurosurgery 2009;65:A29-43.
13. Ranzenberger LR, Snyder T. Diffusion Tensor Imaging. In: StatPearls. Treasure Island (FL): StatPearls Publishing, 2022.
14. Cheng SJ, Tsai PH, Lee YT, Li YT, Chung HW, Chen CY. Diffusion Tensor Imaging of the Spinal Cord. Magn Reson Imaging Clin N Am 2021;29:195-204.
15. Khalilzadeh O, Fayad LM, Ahlawat S. 3D MR Neurography. Semin Musculoskelet Radiol 2021;25:409-17.

16. Boecker AH, Lukhaup L, Aman M, Bergmeister K, Schwarz D, Bendszus M, Kneser U, Harhaus L. Evaluation of MR-neurography in diagnosis and treatment in peripheral nerve surgery of the upper extremity: A matched cohort study. Microsurgery 2022;42:160-9.
17. Hansen B, Jespersen SN. Recent Developments in Fast Kurtosis Imaging. Front Phys 2017;5:40.
18. Andersson G, Orädd G, Sultan F, Novikov LN. In vivo Diffusion Tensor Imaging, Diffusion Kurtosis Imaging, and Tractography of a Sciatic Nerve Injury Model in Rat at 9.4T. Sci Rep 2018;8:12911.
19. Sheikh KA. Non-invasive imaging of nerve regeneration. Exp Neurol 2010;223:72-6.
20. Manzanera Esteve IV, Farinas AF, Pollins AC, Nussenbaum ME, Cardwell NL, Kahn H, Does MD, Dortch RD, Thayer WP. Noninvasive diffusion MRI to determine the severity of peripheral nerve injury. Magn Reson Imaging 2021;83:96-106.
21. Pridmore MD, Glassman GE, Pollins AC, Manzanera Esteve IV, Drolet BC, Weikert DR, Does MD, Perdikis G, Thayer WP, Dortch RD. Initial findings in traumatic peripheral nerve injury and repair with diffusion tensor imaging. Ann Clin Transl Neurol 2021;8:332-47.
22. Marquez Neto OR, Leite MS, Freitas T, Mendelovitz P, Villela EA, Kessler IM. The role of magnetic resonance imaging in the evaluation of peripheral nerves following traumatic lesion: where do we stand?. Acta Neurochir (Wien) 2017;159:281-90.
23. van Rosmalen MHJ, Goedee HS, Derks R, Asselman FL, Verhamme C, de Luca A, Hendrikse J, van der Pol WL, Froeling M. Quantitative magnetic resonance imaging of the brachial plexus shows specific changes in nerve architecture in chronic inflammatory demyelinating polyneuropathy, multifocal motor neuropathy and motor neuron disease. Eur J Neurol 2021;28:2716-26.
24. Yeh FC, Wedeen VJ, Tseng WY. Generalized q-sampling imaging. IEEE Trans Med Imaging 2010;29:1626-35.
25. Yeh FC, Zaydan IM, Suski VR, Lacomis D, Richardson RM, Maroon JC, Barrios-Martinez J. Differential tractography as a track-based biomarker for neuronal injury. Neuroimage 2019;202:116131.
26. Yeh FC, Liu L, Hitchens TK, Wu YL. Mapping immune cell infiltration using restricted diffusion MRI. Magn Reson Med 2017;77:603-12.
27. Garic D, Yeh FC, Graziano P, Dick AS. In vivo restricted diffusion imaging (RDI) is sensitive to differences in axonal density in typical children and adults. Brain Struct Funct 2021;226:2689-705.
28. Shen CY, Tyan YS, Kuo LW, Wu CW, Weng JC. Quantitative Evaluation of Rabbit Brain Injury after Cerebral Hemisphere Radiation Exposure Using Generalized q-Sampling Imaging. PLoS One 2015;10:e0133001.
29. Jeon T, Fung MM, Koch KM, Tan ET, Sneag DB. Peripheral nerve diffusion tensor imaging: Overview, pitfalls, and future directions. J Magn Reson Imaging 2018;47:1171-89.
30. Bruno F, Arrigoni F, Mariani S, Patriarca L, Palumbo P, Natella R, Ma L, Guglielmi G, Galzio RJ, Splendiani A, Di Cesare E, Masciocchi C, Barile A. Application of diffusion tensor imaging (DTI) and MR-tractography in the evaluation of peripheral nerve tumours: state of the art and review of the literature. Acta Biomed 2019;90:68-76.
31. Heckel A, Weiler M, Xia A, Ruetters M, Pham M, Bendszus M, Heiland S, Baeumer P. Peripheral Nerve Diffusion Tensor Imaging: Assessment of Axon and Myelin Sheath Integrity. PLoS One 2015;10:e0130833.
32. Su X, Kong X, Alwalid O, Wang J, Zhang H, Lu Z, Zheng C. Multisequence Quantitative Magnetic Resonance Neurography of Brachial and Lumbosacral Plexus in Chronic Inflammatory Demyelinating Polyneuropathy. Front Neurosci 2021;15:649071.
33. Yeh FC, Verstynen TD, Wang Y, Fernández-Miranda JC, Tseng WY. Deterministic diffusion fiber tracking improved by quantitative anisotropy. PLoS One 2013;8:e80713.
34. Yeh FC, Wedeen VJ, Tseng WY. Estimation of fiber orientation and spin density distribution by diffusion deconvolution. Neuroimage 2011;55:1054-62.
35. Ibrahim I, Škoch A, Herynek V, Jírů F, Tintěra J. Magnetic resonance tractography of the lumbosacral plexus: Step-by-step. Medicine (Baltimore) 2021;100:e24646.
36. Holm S. A simple sequentially rejective multiple test procedure. Scand J Stat 1979;6:65-70.
37. Keller S, Wang ZJ, Golsari A, Kim AC, Kooijman H, Adam G, Yamamura J. Feasibility of peripheral nerve MR neurography using diffusion tensor imaging adapted to skeletal muscle disease. Acta Radiol 2018;59:560-8.
38. Ho MJ, Manoliu A, Kuhn FP, Stieltjes B, Klarhöfer M, Feiweier T, Marcon M, Andreisek G. Evaluation of Reproducibility of Diffusion Tensor Imaging in the Brachial Plexus at 3.0 T. Invest Radiol 2017;52:482-7.
39. Oudeman J, Verhamme C, Engbersen MP, Caan MWA, Maas M, Froeling M, Nederveen AJ, Strijkers GJ. Diffusion tensor MRI of the healthy brachial plexus. PLoS One 2018;13:e0196975.
40. Wade RG, Whittam A, Teh I, Andersson G, Yeh FC,

Wiberg M, Bourke G. Diffusion tensor imaging of the roots of the brachial plexus: a systematic review and meta-analysis of normative values. Clin Transl Imaging 2020;8:419-31.
41. Zhang H, Wang Y, Lu T, Qiu B, Tang Y, Ou S, Tie X, Sun C, Xu K, Wang Y. Differences between generalized q-sampling imaging and diffusion tensor imaging in the preoperative visualization of the nerve fiber tracts within peritumoral edema in brain. Neurosurgery 2013;73:1044-53; discussion 1053.
42. van der Jagt PK, Dik P, Froeling M, Kwee TC, Nievelstein RA, ten Haken B, Leemans A. Architectural configuration and microstructural properties of the sacral plexus: a diffusion tensor MRI and fiber tractography study. Neuroimage 2012;62:1792-9.
43. Naraghi AM, Awdeh H, Wadhwa V, Andreisek G, Chhabra A. Diffusion tensor imaging of peripheral nerves. Semin Musculoskelet Radiol 2015;19:191-200.
44. Kollmer J, Bendszus M. Magnetic Resonance Neurography: Improved Diagnosis of Peripheral Neuropathies. Neurotherapeutics 2021;18:2368-83.
45. Mazal AT, Faramarzalian A, Samet JD, Gill K, Cheng J, Chhabra A. MR neurography of the brachial plexus in adult and pediatric age groups: evolution, recent advances, and future directions. Expert Rev Med Devices 2020;17:111-22.
46. Sneag DB, Daniels SP, Geannette C, Queler SC, Lin BQ, de Silva C, Tan ET. Post-Contrast 3D Inversion Recovery Magnetic Resonance Neurography for Evaluation of Branch Nerves of the Brachial Plexus. Eur J Radiol 2020;132:109304.
47. Zhai H, Lv Y, Kong X, Liu X, Liu D. Magnetic resonance neurography appearance and diagnostic evaluation of peripheral nerve sheath tumors. Sci Rep 2019;9:6939.
48. Su X, Kong X, Lu Z, Zhou M, Wang J, Liu X, Kong X, Zhang H, Zheng C. Use of Magnetic Resonance Neurography for Evaluating the Distribution and Patterns of Chronic Inflammatory Demyelinating Polyneuropathy. Korean J Radiol 2020;21:483-93.
49. Xu Z, Zhang T, Chen J, Liu Z, Wang T, Hu Y, Zhang J, Xue F. Combine contrast-enhanced 3D T2-weighted short inversion time inversion recovery MR neurography with MR angiography at 1.5 T in the assessment of brachial plexopathy. MAGMA 2021;34:229-39.

Cite this article as: Ibrahim I, Škoch A, Herynek V, Humhej I, Beran J, Flusserová V, Rolencová E, Juhaňáková M, Brzák M, Nagy M, Tintěra J. Magnetic resonance tractography of the brachial plexus: step-by-step. Quant Imaging Med Surg 2022;12(9):4488-4501. doi: 10.21037/qims-22-30

